Streaking and Wigner time delays in photoemission from atoms and surfaces

C.-H. Zhang and U. Thumm
Department of Physics, Kansas State University, Manhattan, Kansas 66506, USA
(Received 7 June 2011; published 1 September 2011)

Streaked photoemission metrology allows the observation of an apparent relative time delay between the detection of photoelectrons from different initial electronic states. This relative delay is obtained by recording the photoelectron yield as a function of the delay between an ionizing ultrashort extended ultraviolet pulse and a streaking infrared (IR) pulse. Theoretically, photoemission delays can be defined based on (i) the phase shift the photoelectron wave function accumulates during the release and propagation of the photoelectron ("Wigner delay") and, alternatively, (ii) the streaking trace in the calculated photoemission spectrum ("streaking delay"). We investigate the relation between Wigner and streaking delays in the photoemission from atomic and solid-surface targets. For solid targets and assuming a vanishing IR skin depth, both Wigner and streaking delays can be interpreted as an average propagation time needed by photoelectrons to reach the surface, while the two delays differ for nonvanishing skin depths. For atomic targets, the difference between Wigner and streaking delays depends on the range of the ionic potential.

DOI: 10.1103/PhysRevA.84.033401 PACS number(s): 42.65.Re

I. INTRODUCTION

Streaked photoemission spectroscopy is increasingly applied to resolve ultra-fast electronic processes at the natural time scale ($\approx$1 atomic unit $= 2.4 \times 10^{-17}$ s $= 24$ as) of the motion of valence electrons in matter. Streaking metrology uses ultra-short pulses of extreme ultraviolet (XUV) radiation to emit electrons into the electric field of a delayed infrared (IR) laser pulse. The XUV and IR pulses in this pump-probe setup are phase coherent, and the yield of emitted photoelectrons is recorded as a function of the delay Δt between the two pulses [1]. The resulting energy-resolved photoemission spectra show stripes that oscillate in Δt with the period of the IR-laser electric field. These streaking traces occur in distinct photoelectron kinetic energy intervals that are determined by the spectral width of the XUV pulse, the IR-laser intensity, and the density of states of the target. For photoemission out of energetically resolved discrete atomic levels, streaking traces can be related to a given initial state, while for photoemission from electronic states in solids they are modulated by the density of states within a given band of occupied states. The analysis of streaked photoemission spectra proceeds by fitting the center of energy (COE) of a given streaking trace as a function of Δt to a sine function with an adjustable phase, thereby mapping energy shifts induced by the IR laser onto a time delay between the apparent release of the photoelectron and the arrival of the XUV pulse [2,3].

Streaked photoelectron spectra from localized states of atomic targets [4] and both delocalized conduction band (CB) and localized core-level bands of solids [2] have recently been recorded, leading to an ongoing debate about (i) the interpretation of the deduced photoemission time delays and (ii) the possibility of distinguishing delay contributions from the primary XUV-photorelease process and subsequent photoelectron propagation in the ionic potential of the target and the streaking IR-laser electric field [5–8]. Applying streaking metrology to neon atoms, Schultze *et al.* [4] measured a *relative* photoemission streaking delay of $\Delta\tau_S = 21 \pm 5$ as for the release of electrons from $2p$ orbitals relative to emission from $2s$ orbitals. The authors analyzed their measured relative delay in terms of the relative Wigner delay $\Delta\tau_W(\epsilon)$, which is given by the energy derivative of the spectral phase of the calculated photoelectron wave function [9,10], and averaged $\Delta\tau_W(\epsilon)$ over the spectral profile of the XUV pulse. The difference between their calculated averaged relative Wigner delays $\overline{\Delta\tau}_W$ for emission from the $2s$ and $2p$ orbitals did not exceed $\overline{\Delta\tau}(2p-2s) = \overline{\tau}_W(2p) - \overline{\tau}_W(2s) = 6.4$ as, even for calculations that included electronic correlation in neon at the multiconfiguration-Hartree-Fock level. The authors linked the mismatch between their measured relative streaking and calculated Wigner delays to the extreme sensitivity of the photoelectron wave function's spectral phase to electronic correlation effects in multielectron atoms.

The same experiment [4] was subsequently analyzed by Kheifets and Ivanov [5] based on numerical solutions of the time-dependent Schrödinger equation (TDSE) for a single active electron moving in the Hartree-Fock potential of a Ne^+ ion and, in a separate approach, by including electronic correlation effects to some extent by numerically solving a set of coupled equations in a random-phase-approximation-with-exchange model. These calculations reproduce only less than one half of the measured relative delay of 21 as, and the authors speculated that the much larger observed relative delay might not be due solely to the XUV-induced release process, even if electronic correlation effects were accurately accounted for. The measured relative streaking delay might thus include significant contributions from the photoelectron's interaction with the streaking IR-laser electric field. Indeed, the single-electron TSDE calculations by Ivanov [7] showed that the IR electric field has a considerable influence on the Wigner delay for photoemission. The question then arises whether this IR-dressed Wigner delay can be used to interpret the measured relative streaking delay. As shown in our previous investigation of time-resolved photoemission from a one-dimensional (1D) model hydrogen atom [6], the streaking delay is independent of the IR-laser intensity. This was confirmed recently in a full-dimensionality calculation for atoms by Nagele *et al.* [8].

Investigating photoemission from a tungsten surface, Cavalieri *et al.* [2] have measured a relative streaking

delay of $\Delta\tau_S(\mathrm{CB}-4f)=\tau_S(\mathrm{CB})-\tau_S(4f)=110\pm70$ as for electrons emitted from $4f$ core levels relative to electrons released from the CB. This relative delay was interpreted as the delayed onset of IR streaking, i.e., as the difference in time needed by $4f$ and CB electrons to reach the surface [2,11]. However, as we will argue in Sec. III B, this interpretation is only valid under the assumption that the streaking IR field is fully screened inside the solid. We will also show in this work that Wigner and streaking delays become identical only in this limit of a sudden onset of IR streaking at the surface. We will show that the streaking delay sensitively depends on the IR skin depth δ_L. Therefore, the intuitive interpretation of relative streaking delays in terms of an effective photoelectron path length inside the solid becomes questionable for realistic values of δ_L, depending on how exactly the IR electric field becomes screened in the solid.

While only relative streaking delays can be deduced from measured photoemission spectra, Wigner time delays are conveniently derived from calculated photoelectron wave functions. Wigner and streaking delays in time-resolved atomic photoemission were examined recently [7,8], and the nature of delays within the general context of scattering, decay, and photo- and particle-induced emission processes in atomic, nuclear, and other branches of physics has been discussed by theorists for more than half a century [9,10] (for a recent review see [12].) In this work, we investigate the relation between Wigner and streaking delays for photoemission from atoms in the gas phase and solid surfaces. In Sec. II, we present the underlying theoretical models and our schemes for calculating time delays in photoemission. In Sec. III, we compare and discuss our numerical results of time-resolved photoemission spectra from atoms (Sec. III A) and core-level and conduction bands of solid targets (Sec. III B). In particular, we investigate the dependence of the corresponding time delays on the XUV photon energy, the effective range z_c of the atomic model potential, the initial state, the IR skin depth, and the position of the Fermi level. Our conclusions follow in Sec. IV. Unless indicated otherwise, we use atomic units (a.u.) throughout this work.

II. DEFINITION AND COMPUTATION OF WIGNER AND STREAKING TIME DELAYS

The essence of the time delay introduced by Wigner and Smith [9,10] can be understood for the elementary example of potential scattering in one spatial dimension, by representing the projectile as an incident wave packet

$$\delta\psi_{\mathrm{in}}(z,t)=\int dk a_k e^{ikz-i\varepsilon_k t} \tag{1}$$

in terms of a superposition with amplitudes a_k of plane waves with momenta k centered about k_c and energies ε_k. Scattering subject to the projectile-target-interaction potential V of finite range results in the outgoing wave

$$\delta\psi_{\mathrm{out}}(z,t)=\int dk a_k e^{i\varphi_k}e^{ikz-i\varepsilon_k t}, \tag{2}$$

for which each spectral component is phase shifted by φ_k relative to the corresponding component of the incident wave. Depending on the values of the scattering phase shifts φ_k, wave fronts of the scattered wave are shifted relative to the incident wave. The phase shifts φ_k thus quantify the effect of V on $\delta\psi_{\mathrm{in}}$. Depending on the nature of V, wave fronts of all plane-wave components and the center and crest of the scattered wave packet may appear behind or ahead of the corresponding terms of the incident wave packet. The scattered wave packet can thus be characterized by a positive or negative delay time τ, depending on whether its wave fronts or center are detected after or before they would be detected in the absence of V, respectively. More precisely, the phase shifts of individual traveling plane wave components lead to spectral delays

$$\tau_W(\varepsilon_k)=\frac{\partial\varphi_k}{\partial\varepsilon_k}, \tag{3}$$

which, evaluated at the spectral center $\varepsilon_c=k_c^2/2$ of the incident wave packet, define the Wigner delay [9,10]

$$\tau_W^{\mathrm{I}}=\tau_W(\varepsilon_c). \tag{4}$$

An alternative method for assessing the delay of the scattered relative to the incident wave packet is given in terms of the expectation values for the position,

$$\langle z\rangle(t)=\int_0^\infty dz z|\delta\psi_{\mathrm{out}}(z,t)|^2, \tag{5}$$

and velocity,

$$\langle v\rangle=\int_0^\infty dk|k|\delta\phi_{\mathrm{out}}(k,t)|^2, \tag{6}$$

of the scattered wave packet at a sufficiently large time $t>T$ after the interaction according to [12,13]

$$\langle z\rangle=\langle v\rangle(t-\tau_W^{\mathrm{II}}), \tag{7}$$

where $\delta\phi_{\mathrm{out}}(k,t)$ is the Fourier transformation of $\delta\psi_{\mathrm{out}}(z,t)$. The time T is chosen so that $V[\langle z\rangle(t)]\sim0$ and all spectral phases φ_k and $\langle v\rangle$ of the outgoing wave packet remain time independent to a very good approximation for $t>T$. This fitting procedure can be understood classically by identifying the expectation values for position and velocity in Eq. (7) with the motion of a point particle (Fig. 1). We refer to both τ_W^{I} and τ_W^{II} as "Wigner delay" since it can be shown [12] that they are closely related by the expression

$$\tau_W^{\mathrm{II}}=\int dk|\delta\phi_{\mathrm{out}}(k,t)|^2\tau_W^{\mathrm{I}}(\varepsilon_k). \tag{8}$$

Indeed, our numerical results in Sec. III will confirm that τ_W^{I} and τ_W^{II} are almost identical.

Both definitions of the Wigner time delay, τ_W^{I} and τ_W^{II}, have been used to characterize scattering processes [12] and can also be applied to determine delays in photoemission. They were recently used to interpret the relative delay in the IR-streaked XUV spectra from the $2s$ and $2p$ shells in neon [4,5,7]. We thus believe that it is important to carefully investigate the relation between the Wigner and streaking delays.

We calculate the two Wigner delays for photoionization by solving the TDSE for photoelectron wave packets $\delta\psi(z,t)$ emitted from an initial state $\psi_i(z,t)$ [6],

$$i\frac{\partial}{\partial t}\delta\psi(z,t)=\left[-\frac{p^2}{2}+V(z)\right]\delta\psi(z,t)+zE_X(t)\psi_i(z,t), \tag{9}$$

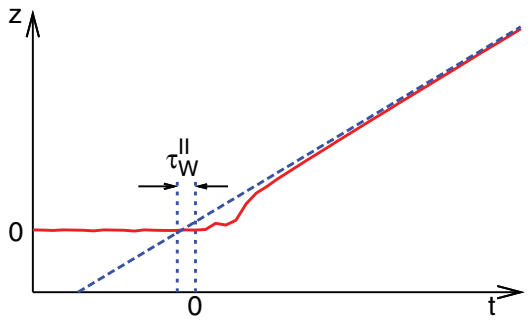

FIG. 1. (Color online) Interpretation of the Wigner delay in the photoionization of atoms. The solid line shows schematically the expectation values for the position $\langle z\rangle$ of the photoelectron wave packet. The photoemission Wigner delay τ_W^{II} is determined by a straight-line extrapolation of $\langle z\rangle$ according to Eq. (7) (dashed line). The XUV pulse is centered at $t = 0$.

where $p = id/dz$ is the momentum operator, and $\psi_i(z,t) = e^{i|\varepsilon_B|t}\psi_i(z)$ is the stationary initial state with binding energy ε_B. For convenience we drop the subscript "out" and designate the outgoing photoelectron wave simply as $\delta\psi(z,t)$. We consider photoemission by an attosecond XUV pulse from either the ground state of a 1D model atom or from the energetically lowest bands of occupied initial states in the periodic 1D model potential of a solid. For the atomic case, we choose $\psi_i(z,t)$ to be the ground state of the model atom with a potential $V(z)$. For photoemission from a surface, $\psi_i(z,t)$ designates Bloch waves from within a given band with Bloch momenta k_i.

We represent the coupling of the XUV pulse electric field E_X to the electron in the dipole-length form and assume a Gaussian pulse profile,

$$E_X(t) \sim e^{-2\ln 2(t/\tau_X)^2}\sin(\omega_X t). \tag{10}$$

We assume a pulse duration $\tau_X = 300$ as and a variable central frequency ω_X.

We propagate the photoelectron wave packet from -4 to 8 fs on a spatial grid that extends over 32,000 a.u. and calculate the Wigner delays $\tau_W^{I,II}$ according to (4) and (7). Rewriting the photoelectron wave packet at the large time $T \gg \tau_X$ as [6,7]

$$\delta\psi(z,t=T) \sim \int dk\,\psi_k(z)d_k\tilde{E}_X(\varepsilon_k-\varepsilon_B)e^{-i\varepsilon_k T}, \tag{11}$$

where $\psi_k(z)$ is a continuum eigenstate in the potential $V(z)$ with energy ε_k, $d_k = \langle\psi_k|z|\psi_i\rangle$ is the dipole matrix element, and $\tilde{E}_X(\omega) = \int dt\,E_X(t)e^{i\omega t}$ is the spectrum of $E_X(t)$, demonstrates that the Wigner delays depend on both the electron release during the dipole coupling of the XUV electric field and the propagation of the photoelectron in the continuum.

In order to calculate streaking delays from the streaked photoemission spectra, the influence of the streaking IR-laser field on the active electron needs to be investigated. The IR streaking effect on the release and propagation of the photoelectron is included by replacing p with $p + A_L(z,t-\Delta t)$ in Eq. (9). The influence of the IR laser on the initial state can be included by numerically propagating the initial state in the IR-laser electric field according to [6]

$$i\frac{\partial}{\partial t}\psi_i(z,t) = \left\{\frac{1}{2}[p + A_L(z,t-\Delta t)]^2 + V(z)\right\}\psi_i(z,t), \tag{12}$$

where Δt is the delay between the centers of the XUV and IR pulses, and the convention is used that $\Delta t > 0$ corresponds to the XUV pulse preceding the IR pulse. We model the vector potential of the IR-laser pulse as

$$A_L(t) = A_0\sin^2(\pi t/\tau_L)\cos[\omega_L(t-\tau_L/2)] \tag{13}$$

for $0 \leqslant t \leqslant \tau_L$ and set A_L to 0 otherwise. As pulse parameters, we choose the central photon energy $\hbar\omega_L = 1.57$ eV (corresponding to a wavelength of $\lambda_L = 800$ nm), peak intensity $I_L = A_0^2\omega_L^2/2 = 5\times10^{11}$ W/cm^2, and pulse length $\tau_L = 8$ fs.

If free-electron dispersion is assumed ($\varepsilon = k^2/2$), the energy-differential photoemission probability is given by

$$P(\varepsilon,\Delta t) = \frac{1}{k}|\delta\phi(k,\infty;\Delta t)|^2, \tag{14}$$

where $\delta\phi(k,\infty;\Delta t)$ is the Fourier transform of $\delta\psi(z,t\to\infty;\Delta t)$. The XUV-IR delay-dependent COE for a given streaking trace is [3]

$$E_{\rm COE}(\Delta t) = \frac{1}{2P_{\rm tot}(\Delta t)}\int dk|k\,\delta\phi(k,\infty;\Delta t)|^2, \tag{15}$$

with the total emission probability

$$P_{\rm tot}(\Delta t) = \int dk|\delta\phi(k,\infty;\Delta t)|^2. \tag{16}$$

After calculating $E_{\rm COE}(\Delta t)$ for a range of XUV-IR delays $-\tau_L/2 \leqslant \Delta t \leqslant \tau_L/2$, we obtain the streaking delay τ_S relative to A_L by fitting the parameters a, b, and τ_S to the expression [3,6]

$$E_{\rm COE}(\Delta t) = a + bA_L(\Delta t - \tau_S). \tag{17}$$

For XUV photoemission from solids, Eqs. (14)–(17) remain valid. In this case, the initial states in Eq. (9) are individual Bloch waves with momenta in the first Brillouin zone of either core-level or conduction band. We will show in Sec. III B how to calculate band-averaged results.

III. NUMERICAL RESULTS

A. One-dimensional model hydrogen atom

In this section, we discuss our numerical results for Wigner and streaking delays for XUV photoemission from the ground state with binding energy $\varepsilon_B = 13.6$ eV of the soft-core Coulomb potential

$$V(z) = V_c(z) = -1/\sqrt{z^2+2}. \tag{18}$$

In the calculation of the Wigner delay τ_W^{I}, the direct numerical determination of the phase of the photoelectron wave packet according to $\varphi_k = \ln\delta\phi(k,T)/|\delta\phi(k,T)|$ is inaccurate or impossible for values of k where $|\delta\phi(k,T)|$ is extremely small. Furthermore, ε_c is difficult to determine from $\delta\phi(k,T)$ [see Fig. 2(a)]. In order to overcome these two difficulties, we fit the real part $\mathrm{Re}[\delta\phi(k,T)]$ of the calculated photoelectron wave packet to the function

$$f(\varepsilon) = Ae^{-2\ln 2[(\varepsilon-\varepsilon_c)/\Delta\varepsilon]^2}\cos(\varphi_k), \tag{19}$$

with

$$\varphi_k = \alpha(\varepsilon-\varepsilon_c) + \beta(\varepsilon-\varepsilon_c)^2 + \gamma, \tag{20}$$

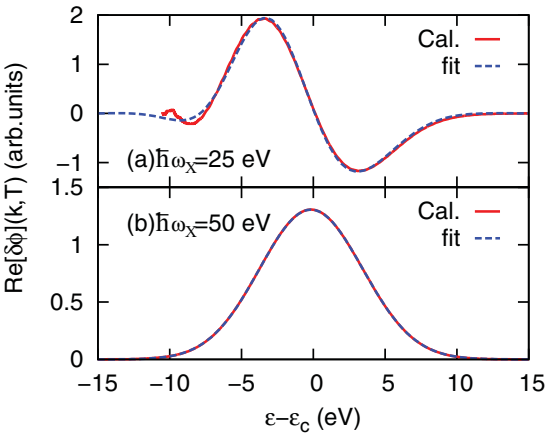

FIG. 2. (Color online) Real part of the calculated and the fitted momentum-space photoelectron wave packets for ionization from 1D model hydrogen atoms by XUV pulses with energies of (a) 25 eV and (b) 50 eV.

and determine (by least-squares fit over a large range of $\varepsilon = k^2/2$ values) the parameters ε_c, $\Delta\varepsilon$, $\alpha = \tau_W^{\mathrm{I}}$, β, and γ. As shown in Fig. 2 for photoionization with $\hbar\omega_X = 25$ and 50 eV, the spectra of the calculated (by numerically solving the TDSE) and fitted photoelectron wave packets are in excellent agreement. Since according to Eq. (11) the XUV pulse spectral profile is imprinted on the photoelectron wave packet, we find that the fitted values $\Delta\varepsilon(\hbar\omega_X = 25\ \mathrm{eV}) = 5.96$ eV and $\Delta\varepsilon(\hbar\omega_X = 50\ \mathrm{eV}) = 6.11$ eV are close to the spectral width $\hbar\Delta\omega_X = 6.08$ eV of the XUV pulse.

Figure 3 shows the Wigner delays $\tau_W^{\mathrm{I,II}}$ for the 1D model hydrogen atom, calculated according to Eqs. (7) and (19) and (20), in comparison with the streaking delay τ_S, calculated as described in Sec. II [6]. All delays are negative. The two Wigner delays are almost identical and their absolute values are much larger than the streaking delay. Having established that the two Wigner delays almost coincide for all parameters considered in this work, we only show results for τ_W^{II} from now on and drop the superscript "II" for convenience, unless noted otherwise. In order to investigate the difference between the Wigner and streaking delays, we modify the infinite range of

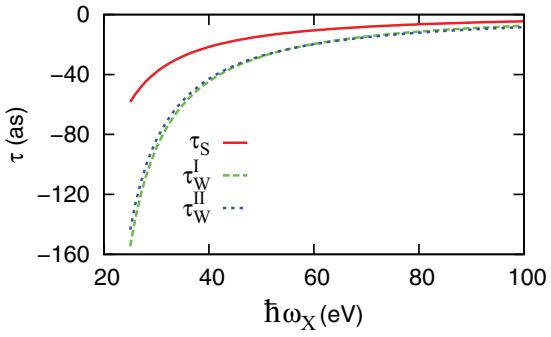

FIG. 3. (Color online) Comparison of the Wigner delays $\tau_W^{\mathrm{I,II}}$ and the streaking delay τ_S for photoionization of 1D model hydrogen atoms as a function of the XUV photon energy $\hbar\omega_X$.

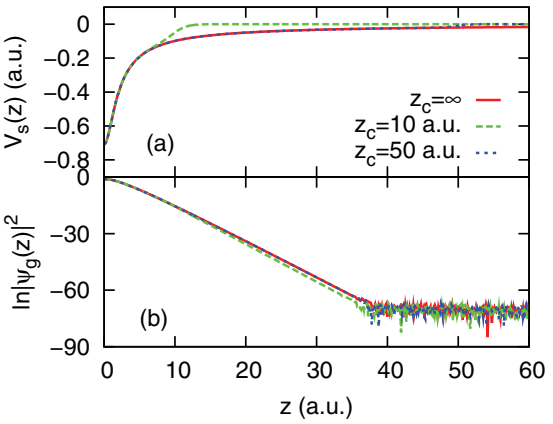

FIG. 4. (Color online) The modified Coulomb potential (21) (a) and its ground-state wave function (b) for three different interaction ranges z_c.

the potential Eq. (18) with a Wood-Saxon factor,

$$V_s(z) = V_c(z)\left[1 - \frac{1}{1 + e^{-(|z|-z_c)/a}}\right]. \tag{21}$$

The range of $V_s(z)$ is controlled by z_c. The parameter a defines the lengths over which $V_c(z)$ is screened to approach zero. In our calculation, we use $a = 1$. For $z_c \to \infty V_s$ converges to V_c [Fig. 4(a)]. We numerically verified that for values of z_c larger than a few atomic units, the ground-state wave function and energy in $V_s(z)$ are practically independent of z_c [Fig. 4(b)].

In Fig. 5 and Table I we compare the Wigner and streaking delays at three different ranges z_c. The comparison shows that for an interaction range slightly larger than the extent of the ground-state probability distribution, say, $z_d \sim 2$, the Wigner and streaking delays coincide [see Fig. 5(a)]. In contrast, for $z_c \gg z_d$, $|\tau_W| > |\tau_S|$, and both delays approach their values for the 1D model potential, Eq. (18). In this case the difference of the two delays is largest at lower photoelectron kinetic energies [Figs. 5(b) and 5(c)]. The comparison of the three graphs also

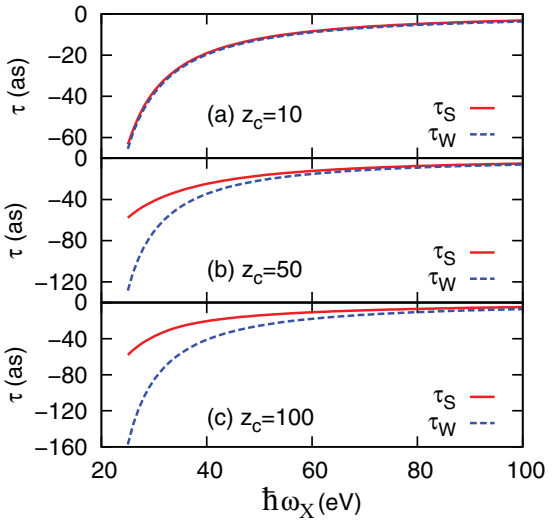

FIG. 5. (Color online) Comparison of the Wigner delay τ_W and the streaking delay τ_S for three interaction ranges z_c in Eq. (21) as a function of the XUV photon energy $\hbar\omega_X$.

TABLE I. Streaking and Wigner time delays from Fig. 5 for three range parameters z_c and three XUV photon energies $\hbar\omega_X$.

$\hbar\omega_X$ (eV)	z_c (a.u.)	τ_S (as)	τ_W (as)
30	10	−37	−38
	50	−41	−71
	100	−37	−85
50	10	−12	−12
	50	−17	−22
	100	−14	−26
70	10	−6	−7
	50	−9	−11
	100	−8	−13

shows that the Wigner delay is more sensitive to changes in z_c than the streaking delay.

We emphasize that Wigner delays are calculated without including the action of an IR-laser pulse, which might give rise to the question of whether we should instead compare the streaking delay with the Wigner delay obtained in the same IR field, as mentioned in the introduction. Obviously, inclusion of the IR-laser electric field would change the Wigner delay [7]. In this case the photoelectron velocity in Eq. (7) would depend on the XUV-IR delay Δt, and the use of this equation would determine a Wigner delay $\tau_W^{\rm II}$ that varies with Δt and the IR-pulse intensity. The streaking delay, in contrast, does not depend on Δt. It also does not depend on the intensity of the streaking laser, if its intensity is sufficiently low [3,6,8]. Therefore, it is only meaningful to compare streaking delays with IR-field-free Wigner delays. We note that, even though our results do not explain the measured relative streaking delay between photoemission from the $2s$ and $2p$ core levels of neon in the work of Schultze *et al.* [4], our calculations do suggest that the measured relative streaking delay between them is different from the theoretical relative Wigner delay because of the long-ranged Coulomb interaction of the photoelectron with the residual ion.

By computing photoemission spectra and streaking delays with and without including the IR vector potential in Eq. (12), we found that for this atomic target polarization effects of the initial state of the active electron in the electric field of the streaking laser are negligible. This is due to the large energy gap between the ground state and the excited states [6]. With regard to the experiment by Schultze *et al.* [4], we therefore expect initial-state polarization effects to be irrelevant, due the large energy gap of ≈27 eV [14]. In contrast, the initial-state polarization is relevant for the case of photoemission from solid surfaces discussed in the following section.

B. One-dimensional solid

We model the 1D solid surface as a row of N equidistant atomic layers and represent each atom by a Gaussian potential well to form the lattice potential

$$V_{\rm latt}(z) = V_0 - \frac{A_0}{\sqrt{2\pi}\sigma}\sum_{i=1}^{N} e^{-[z+(i+0.5)a_{\rm latt}]^2/(2\sigma^2)}, \qquad (22)$$

where $a_{\rm latt}$ is the lattice constant, σ controls the overlap of the two adjacent atomic potentials, and V_0 and A_0 are chosen to match the known Fermi energy [Fig. 6(a)]. We have oriented the z axis with increasing values toward the vacuum side and put the origin ($z = 0$) at the distance $0.5a_{\rm latt}$ in front of the top nucleus. Diagonalizing the time-independent Schrödinger equation

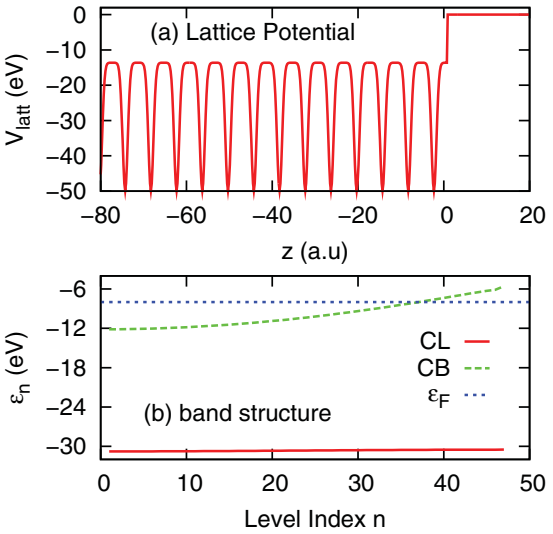

FIG. 6. (Color online) (a) Model lattice potential consisting of equally spaced Gaussian potential wells. (b) Corresponding band structure with one core-level band (CL) and one conduction band (CB). The dotted line indicates the Fermi level ε_F.

$$\varepsilon_n\psi_n(z) = \left[-\frac{1}{2}\frac{d^2}{dz^2} + V_{\rm latt}(z)\right]\psi_n(z) \qquad (23)$$

for $N = 47$, $V_0 = -0.5$, $A_0 = 2$, $a_{\rm latt} = 6$, and $\sigma = 0.1a_{\rm latt}$, we obtain the core-level and conduction-level bands shown in Fig. 6(b). The Fermi energy is $\varepsilon_F = -10.9$ eV.

For the calculation of the XUV photoemission spectrum, we replace $V(z)$ in Eq. (9) by $V_{\rm latt}(z)$ and add the damping term $-iv_z/(2\lambda)$, with the velocity $v_z = \sqrt{2(\omega_X - |\varepsilon_n|)}$, to $V_{\rm latt}(z)$, in order to model scattering of the photoelectrons inside the solid. In a previous study [3], we adjusted the electron mean-free path inside the solid to $\lambda = 5$ Å. This value corresponds to the minimum of the universal curve for λ as a function of the electron's kinetic energy [15]. We continue to use this value for the present investigation. In the calculation of the streaked spectra, we further assume an exponential damping of the IR-laser field inside the solid,

$$A_L(z,t) = A_L(t)[e^{z/\delta_L}\Theta(-z) + \Theta(z)], \qquad (24)$$

characterized by the IR skin depth δ_L.

Within each band, we use the index n to label Bloch wave functions ψ_n with energies ε_n, starting with ε_1 for the lowest energy Bloch wave at the band bottom. Each initial Bloch wave below the Fermi level contributes to the photoemission spectrum with the energy-differential emission probability

$$P_n = P(\varepsilon_n,\Delta t) = \frac{1}{k}|\delta\phi_n(k,\infty;\Delta t)|^2. \qquad (25)$$

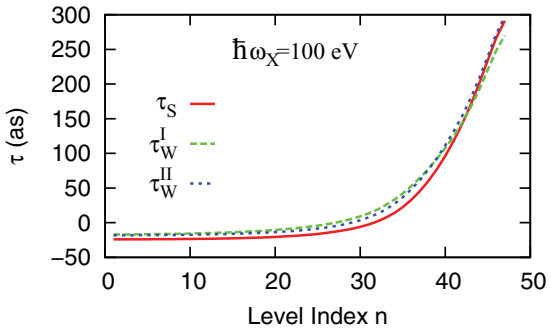

FIG. 7. (Color online) Streaking and Wigner delays, τ_S and $\tau_W^{\mathrm{I,II}}$, for XUV photoemission with $\hbar\omega_X = 100$ eV from the core-level band of a 1D model solid surface as a function of the core-level index n. All delays are computed for the electron mean-free path $\lambda = 5$ Å and no penetration of the IR-laser field into the solid ($\delta_L = 0$) for the streaking delay.

Similarly, each Bloch wave yields to the COE $E_{\mathrm{COE},n}(\Delta t)$, Wigner delays $\tau_{W,n}^{\mathrm{I,II}}$, and streaking delays $\tau_{S,n}$. We first calculate the band-averaged COE,

$$E_{\mathrm{COE}}(\Delta t) = \frac{1}{\sum_n P_n} \sum_{\varepsilon_n < \varepsilon_F} P_n E_{\mathrm{COE},n}(\Delta t), \tag{26}$$

separately for each band. Next we use Eq. (17) to obtain the band-averaged streaking delay τ_S. Similarly, we find the band-averaged Wigner delays according to

$$\tau_W^{\mathrm{I,II}} = \frac{1}{\sum_n P_n} \sum_{\varepsilon_n < \varepsilon_F} P_n \tau_{W,n}^{\mathrm{I,II}}. \tag{27}$$

A comparison of streaking and the two Wigner delays for an XUV photon energy $\hbar\omega_X = 100$ eV and emission from the core-level band is shown in Fig. 7 as a function of the core-level index n. The monotonic increase in level index n in Fig. 7 is just a coincidence. For other energies, these delays do not necessarily increase with n. As for the case of atomic targets (cf., Sec. III A), we find that the difference between the two Wigner delays is negligible. We therefore only present results for τ_W^{II}, which we denote simply as τ_W below. All numerical results shown below are converged in the number of included atomic layers, N.

Wigner and streaking delays as a function of the XUV photon energy $\hbar\omega_X$ for photoemission from three individual core- and three conduction-band Bloch levels are shown in Figs. 8 and 9, respectively. According to its definition in Eq. (7), the Wigner delay can be regarded as an "effective" propagation time for the photoelectron to emerge from the solid. For the special case $\delta_L = 0$, the streaking delay is the travel time photoelectrons need before getting exposed to the streaking IR field outside the solid. Therefore, intuitively, for $\delta_L = 0$ only, one would expect the streaking delay to be almost identical to the Wigner delay. As Figs. 7–10 show, this is confirmed by our numerical results.

It is interesting to observe that, for emission from the core-level band, the band-averaged Wigner and streaking delays decrease monotonically with increasing $\hbar\omega_X$ [Fig. 10(a)]. This decrease closely follows the effective propagation time

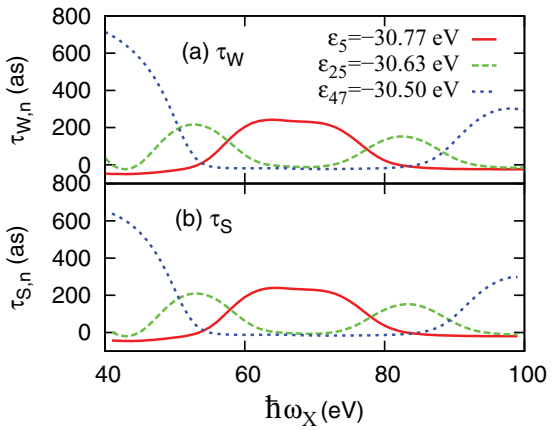

FIG. 8. (Color online) Wigner (a) and streaking (b) time delays for XUV photoemission from three core-level Bloch states with energies ε_5, ε_{25}, and ε_{47} given relative to the ionization limit. Streaking delays are computed for the electron mean-free path $\lambda = 5$ Å and no penetration of the IR-laser field into the solid ($\delta_L = 0$).

$\lambda/\sqrt{2\varepsilon}$ of photoelectrons inside the solid prior to reaching the solid-vacuum interface at $z = 0$, even though delay contributions from individual Bloch levels, τ_n (see Fig. 8), do not show this behavior. This confirms the interpretation that band-averaged Wigner and streaking delays for emission from the core-level band can be regarded as an average time needed for a released photoelectron to travel a distance λ inside the solid [2,11].

However, this interpretation is not valid for photoemission from the CB, where the band-averaged delays behave non-monotonically as a function of $\hbar\omega_X$ as shown in Fig. 10(b). A possible explanation for this difference is the delocalized nature of the CB Bloch wave. This can be checked by examining the core-level-band-averaged delay as a function of the overlap parameter σ in $V_{\mathrm{latt}}(z)$ and will be discussed

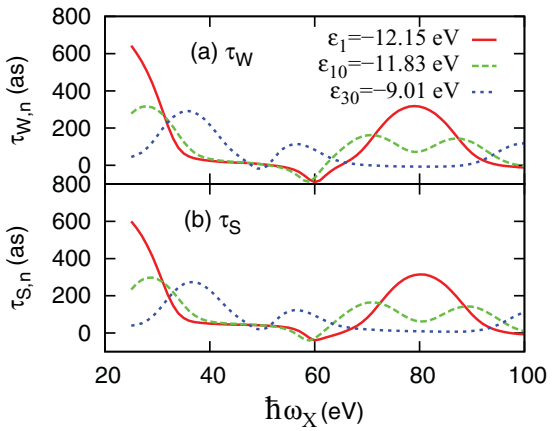

FIG. 9. (Color online) Wigner (a) and streaking (b) time delays for XUV photoemission from three conduction-band levels with energies ε_1, ε_{10}, and ε_{30} given relative to the ionization limit. The occupied part of the conduction band extends from ε_1 to the Fermi level at $\varepsilon_F = -8.22$ eV. Streaking delays are computed for the electron mean-free path $\lambda = 5$ Å and no penetration of the IR-laser field into the solid ($\delta_L = 0$).

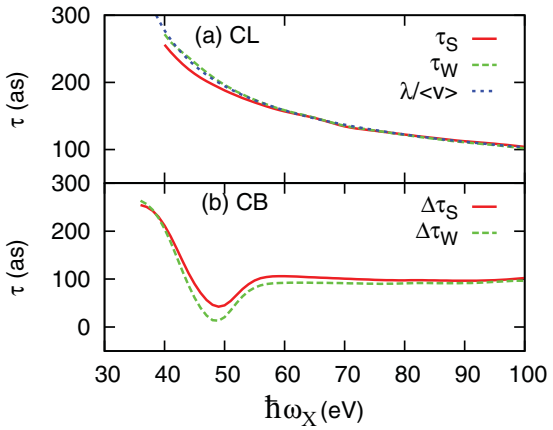

FIG. 10. (Color online) (a) Band-averaged Wigner and streaking delays for XUV photoemission from (a) the conduction band and (b) the core-level band. Streaking delays are computed for the electron mean-free path $\lambda = 5$ Å and no penetration of the IR-laser field into the solid ($\delta_L = 0$).

in a forthcoming publication [16]. This means that, even for $\delta_L = 0$, the relative delays between photoemission from the core-level and CB cannot be due solely to the photoelectron's average travel time in the solid [2,11].

Since (i) the very close correspondence of τ_S and τ_W and (ii) the interpretation of streaking delays in terms of an effective propagation time in the solid are only valid for the special case $\delta_L = 0$, we next investigate the dependence of photoemission delays on the IR skin depth δ_L. Figure 11 shows the band-averaged streaking delay for emission from the core-level band for two XUV photon energies. These results show a very sensitive dependence of τ_S on the IR skin depth, with τ_S changing from positive to negative delays. In contrast to photoemission from the energetically isolated ground states of atoms (Sec. III A), the N Bloch waves form a quasicontinuum and can be easily hybridized in the IR-laser electric field. This initial-state hybridization effect gets stronger the deeper the IR electric field penetrates the solid and accounts for the δ_L dependence of τ_S. We note that the actual IR skin depth is much larger than the electron mean-free

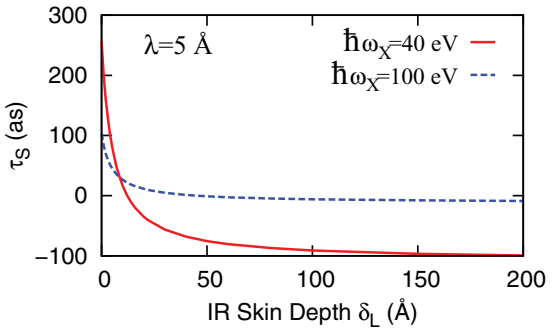

FIG. 11. (Color online) Band-averaged streaking delays for XUV photoemission from the core-level band with photon energies of $\hbar\omega_X = 50$ and 100 eV as a function of the IR-laser skin depth δ_L. The electron mean-free path is $\lambda = 5$ Å.

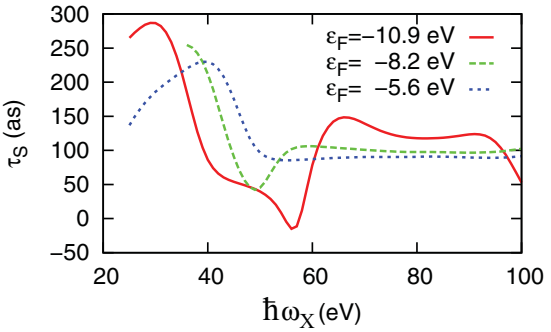

FIG. 12. (Color online) Band-averaged streaking delay in the photoelectron spectrum for photoemission from the conduction band for three values of the Fermi energies ε_F. $\lambda = 5$ Å and $\delta_L = 0$ are used.

path, such that the effective depth over which photoelectrons are assembled is limited by λ, and the IR skin depth tends to become irrelevant for the photocurrent [3]. Accordingly, the photoemission delays in Fig. 11 converge in the limit of large δ_L/λ. We also note that the effective IR-skin depth for photoelectron streaking depends on the direction under which photoelectrons are observed and on the angle of incidence of the IR pulse. In the experiment of Cavalieri *et al.* [2], the angle of incidence of the IR pulse was selected as the Brewster angle, and photoelectrons that are emitted along the surface normal were recorded. For this particular geometry, the normal component of the refracted IR electric field is very small and photoelectron streaking inside the solid becomes negligeable [17].

Another interesting observation, as shown in Fig. 12, is that the band-averaged τ_W and τ_S from the conduction band depend on the position of the Fermi level. Therefore, changing the occupation probability of Bloch waves in the CB, for example, by increasing the temperature or by doping, will change the band-averaged delay. This dependence is absent in the core-level band because all the core levels are below the Fermi level and fully occupied.

IV. CONCLUSIONS

We have examined the relation between Wigner and streaking delays in the XUV photoelectron emission from model atoms and solid surfaces. We showed that both the creation of the photoelectron and its propagation contribute to the Wigner delay. For photoemission from atoms, the two delays are only identical for short-range ionic potentials. For photoemission from surfaces, Wigner and streaking delays become identical only in the limit of no IR-field penetration into the solid, and both delays can be interpreted as the travel time of the photoelectron to the surface. For this case only and for electron emission from the core-level band, both delays can be understood as the average time photoelectrons need to travel a distance equal to the mean-free path in the solid. This interpretation does not hold for photoelectron emission from the conduction band. This dissimilarity is expected to be due to the different (localized versus delocalized) nature of core and conduction-band levels.

We find that streaking delays are very sensitive to changes in the IR skin depth and Fermi energy and deviate from Wigner delays for nonzero IR skin depths. Their dependence on the substrate temperature, impurities, and adsorbate coverage may leave a measurable signature in relative photoemission delays.

ACKNOWLEDGMENTS

This work was supported by the National Science Foundation, Division of Chemical Sciences, Office of Basic Energy Sciences, Office of Energy Research, US Department of Energy. The computing for this project was performed on the Beocat cluster at Kansas State University.

[1] F. Krausz and M. Ivanov, Rev. Mod. Phys. **81**, 163 (2009).
[2] A. L. Cavalieri *et al*., Nature (London) **449**, 1029 (2007).
[3] C.-H. Zhang and U. Thumm, Phys. Rev. Lett. **102**, 123601 (2009); **103**, 239902(E) (2009).
[4] M. Schultze *et al*., Science **328**, 1658 (2010).
[5] A. S. Kheifets and I. A. Ivanov, Phys. Rev. Lett. **105**, 233002 (2010).
[6] C.-H. Zhang and U. Thumm, Phys. Rev. A **82**, 043405 (2010).
[7] I. A. Ivanov, Phys. Rev. A **83**, 023421 (2011).
[8] S. Nagele, R. Pazourek, J. Feist, K. Doblhoff-Dier, C. Lemell, K. Tőkési, and J. Burgdörfer, J. Phys. B **44**, 081001 (2011).
[9] E. P. Wigner, Phys. Rev. **98**, 145 (1955).
[10] F. T. Smith, Phys. Rev. **118**, 349 (1960).
[11] A. K. Kazansky and P. M. Echenique, Phys. Rev. Lett. **102**, 177401 (2009).
[12] C. A. A. de Carvalho and H. M. Nussenzweig, Phys. Rep. **364**, 83 (2002).
[13] W. Brenig and R. Haag, Fortschr. Phys. **7**, 183 (1959).
[14] S. Hüfner, *Photoelectron Spectroscopy*, 3rd ed. (Springer, Berlin, 2003).
[15] A. Zangwill, *Physics at Surfaces* (Cambridge University Press, New York, 1988).
[16] C.-H. Zhang and U. Thumm (submitted for publication).
[17] P. Gibbon, *Short Pulse Laser Interactions with Matter* (Imperial College Press, London, 2005).